Journal of Applied Electrochemistry **34**: 857–866, 2004.
© 2004 *Kluwer Academic Publishers. Printed in the Netherlands.*

Development of an electrodeposited nanomold from compositionally modulated alloys

CHE-YIH LIM[1], Q. HUANG[1], X. XIE[2], A. SAFIR[3], S.A. HARFENIST[2], R. COHN[3] and E.J. PODLAHA[1]*
[1]*Gordon and Mary Cain Department of Chemical Engineering, Louisiana State University, Baton Rouge, LA 70803, USA*
[2]*Geology Department, Louisiana State University, Baton Rouge, LA, USA*
[3]*ElectroOptics Research Institute, University of Louisville, Louisville, KY, USA*
*(*author for correspondence, e-mail: podlaha@lsu.edu)*

Received 20 November 2003; accepted in revised form 19 March 2004

Key words: electrodeposition, multilayers, NiCu/Cu, NiFeCu/Cu, nanoimprinting

Abstract

Electrodeposited multilayers of NiCu/Cu and NiFeCu/Cu were examined for nanoimprinting applications. Layer sizes on the order of 100 nm were deposited and the copper layer etched. Current efficiency and layer composition of electrolytes having different pH values were examined utilizing a rotating disk electrode. Due to large grain growth in the NiCu/Cu system, the bilayers resulted in a macroscopic waviness of the layers. Adding Fe in a small concentration successfully produced straight layers. As an example of the replication technique, the metal multilayer-etched stamp was used to cast the multilayer image in rubber and emboss it in Teflon®.

1. Introduction

The development of an electrodeposited nanomold is of interest in optics and electronics industries for nanoimprinting applications [1–3]. For example, sub-wavelength optics requires lithographic patterning of widths from 50 to 200 nm, where the percentage of stripe width to stripe spacing (duty factor) determines the effective refractive index, and the height of the grating determines the phase retardation. The degree of precision needed is comparable with that achievable by high performance vapor or e-beam deposition systems. The electrodeposition method presented here is a proposed alternative method of producing a master stamper that is less costly and capable of achieving nanometer accuracy and resolution.

Figure 1 illustrates the fabrication of an extremely precise electrodeposited nanostamp, and its application as a nanoimprint master stamper to duplicate the image on a substance. The master stamp is fabricated from the electrodeposition of a compositionally modulated multilayer, with alternating layers having disparate nobilities. After electrodeposition, one layer is selectively etched away to create a relief structure. The nanostamp is subsequently used as a master for casting or embossing a polymeric, ceramic or soft metal material.

Electrodeposition has been widely demonstrated as an effective method to produce multilayers, for example for giant magnetoresistance [4–19] and enhanced hardness [20, 21]. Additionally, etching solutions have been used to preferentially etch large, 100 nm layer sizes of multilayers for scanning electron microscopy (SEM) characterization [21–23]. On a micron scale, the selective etching of layered materials has also been established for lithographically fabricated MicroElectroMechanical Systems [24, 25]. For example, Leith and Schwartz [26] selectively etched an iron-rich NiFe alloy sandwiched between a nickel rich alloy to fabricate a microgear, and to establish conditions for representative microparts. Demonstrated etched regions were approximately 3 μm wide and carried out in an acetic acid solution. Hasegawa et al. [24] and Aria et al. [25] similarly created microstructures by the selective etching of Ni/Cu structures. Either the Cu or Ni layer could be etched in an acidic thiourea solution or a sulfuric acid solution, respectively. However, selective Ni etching required that sulfur be incorporated into the deposit during plating, so that the passivation of Ni was inhibited [25].

In this paper, we present submicron electrodeposited multilayered structures of NiCu/Cu and nickel-rich NiFeCu/Cu alloys. The copper layers are etched preferentially for the creation of a nanometric mold. The effect of the plating electrolyte pH and Cu layer current density on the structure is investigated. An illustrative example of the molding application is presented with representative etched multilayers.

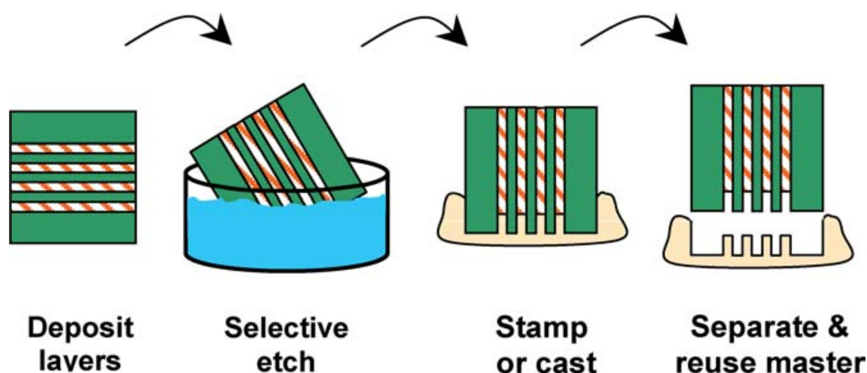

Fig. 1. Fabrication and application of an electrodeposited nanostamp.

2. Experimental details

2.1. *Cell and electrolyte*

A rotating disk cathode was used as the working electrode with a Pt anode. The cathode was a gold plated, stainless steel cylindrical disk with a diameter of 0.6 cm. The rotation rate of the cathode was controlled at a constant 1000 rpm. Deposits were carried out with galvanostatic pulsing with an Amel galvanostat and a Waveteck function generator. The electrolyte was at room temperature and contained the constituents in Table 1, adapted from other literature studies [19, 27, 28].

2.2. *Procedure*

The NiCu/Cu multilayers were pulse-plated onto the rotating disk electrode. The value of the galvanostatic, square-wave pulsed currents were either −3.55, −1.77, or −0.71 mA cm^{-2} for the copper layer and −71.97 mA cm^{-2} for the nickel layer. The electrolyte pH was examined at 2.5, 3.0 and 3.5. Samples were also prepared at pH 3.0 with an additional constituent of 1 g l^{-1} of $FeSO_4 \cdot 7H_2O$ in order to deposit NiFeCu/Cu multilayers. The current density for the Cu- and Ni-rich layers remained the same as for the NiCu/Cu deposits. Pulse plating was carried out with an Amel potentiostat and Waveteck function generator. Polarization curves and ohmic drop were determined using a Bas-Zahner IM6, and the reported potential eliminates the ohmic contribution.

Table 1. Bath composition for NiCu deposition

Constituent	
$NiSO_4 \cdot 6H_2O$	0.115 M
$FeSO_4 \cdot H_2O$	0.0179 M
$CuSO_4 \cdot 5H_2O$	0.001 M
$NaKC_4H_4O_6 \cdot 4H_2O$	0.0266 M
Sulfamic acid	0.0103 M
Sodium saccharin	0.0041 M
Triton X-100	0.6 g/l
pH	Variable

Deposit composition was analyzed with a Kevex Omicron energy-dispersive X-ray fluorescene analyzer. The thickness was analyzed by using a stripping analysis with a Pine Instruments bi-potentionstat to measure the current efficiency (Appendix A). Efficiency was computed by comparing the charge applied to the charge stripped.

Multilayered deposits were analyzed with SEM, JEOL-840A SEM at the Louisiana State University and a LEO 1430 SEM at the University of Louisville. The cross-section of the multilayers was prepared by having the electrodeposited film along with the substrate first embedded in a resin (Sample-Kwick Powder and Liquid, Buehler). Then the sample was cut perpendicularly to the film and further grounded and polished to at least 0.3 μm with diamond pastes. The sample was subsequently etched for 10 s in an aqueous chromic acid–HCl solution given in Table 2, for a short uniform etch, as reported by Bradley and Landolt [29]. Next, the disk was etched in a HNO_3 ethanol solution for 4 min, for the selective etching of Cu. The HNO_3 solution was a mixture of HNO_3 (65%) and C_2H_5OH at a ratio of 4–80 by volume. Lastly, gold was sputtered onto the electrode surface, covering the resin holder and analyzed with SEM.

The mounted sample without a gold coating was used to duplicate the multilayer. A fast-curing two-part silicon rubber (RepliSet-F5, Struers) was placed on the multilayer sample, dried and easily peeled to demonstrate the imaging processes. Embossing into a carbon-impregnated Teflon® was also demonstrated with a press at 1000 psi. Poly(dimethylsiloxane) PDMS was also cast into the multilayered-etched master to reproduce the image. SEM evaluation of the replicate rubber and Teflon® required a coating of sputtered gold.

Table 2. Aqueous solution for the etching process

Components	Quantity
H_2SO_4 (96%)	2 ml
$K_2Cr_2O_7$	1 g
HCl (37%)	0.1 ml

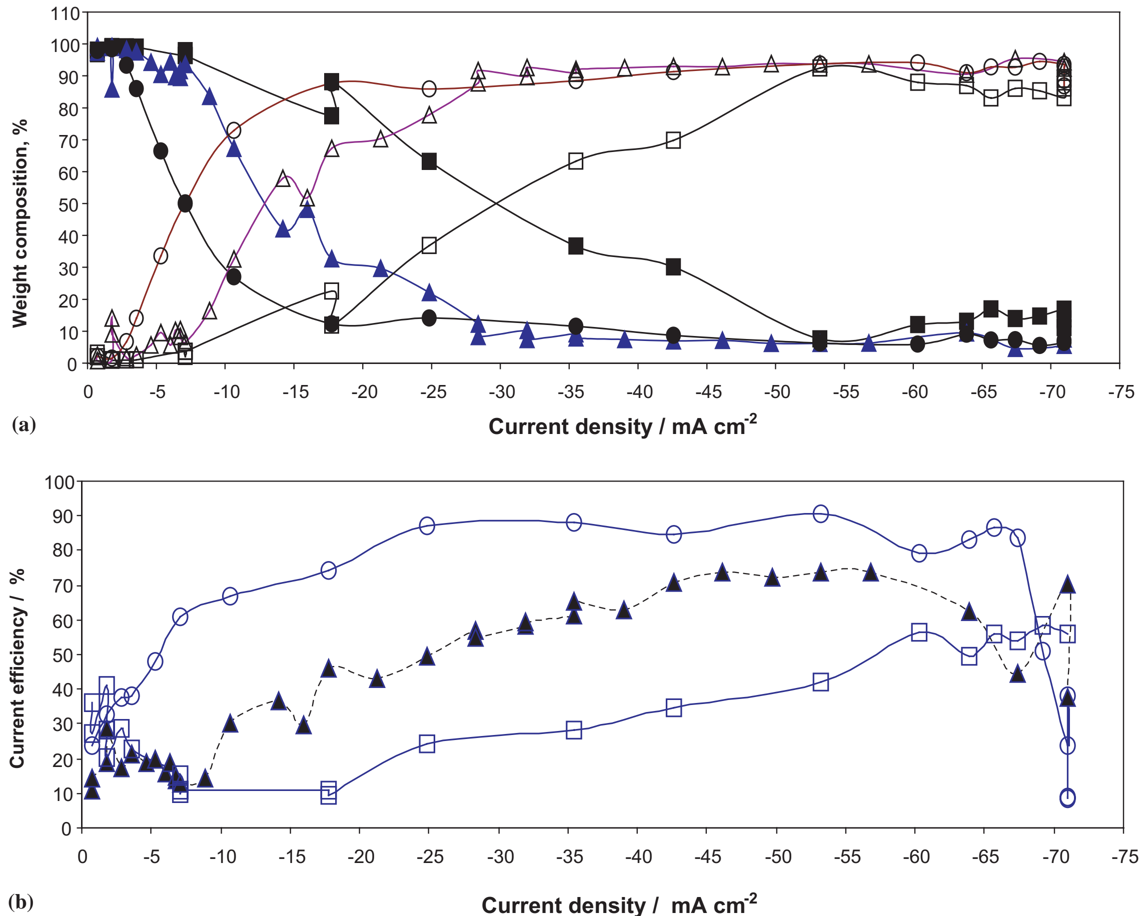

Fig. 2. NiCu (a) deposit composition at pH 2.5, Cu (■), Ni (□); pH 3.0, Cu (▲), Ni (△); and pH 3.5, Cu (●), Ni (○) and (b) current efficiency pH 2.5 (□), pH 3.0 (▲), and pH 3.5 (○).

3. Results and discussions

3.1. *Composition and current density*

Current density values for pulsed multilayer alloy deposition were determined from steady-state DC deposition experiments. Figure 2 shows the NiCu alloy composition and current efficiency for three different pH values. Increasing the pH increased the amount of Ni in the deposit at a given applied current density (Figure 2(a)). At all pH values, the deposits contained more than 90% copper at current densities below -5.0 mA cm^{-2} and contained mostly nickel at -71.97 mA cm^{-2}. The steady state current efficiency is shown in Figure 2(b). In general, the higher the pH the better the efficiency, with exception at the very low and high applied current densities. At current densities below -5 mA cm^{-2} oxygen and proton reduction dominates, while at the high end the evolution of hydrogen from water reduction is significant. During multilayer deposition, it is most desirable to have the largest change in alloy composition between the two nanolayers, which would dictate that deposition occur at these two extremes.

Figure 3 presents the (a) composition and (b) current efficiency obtained from NiFeCu deposits at pH 3.0 electrolytes. The Ni and Cu composition change as a function of applied current density is similar to Figure 2. The small addition of Fe contributes to less than 10% of the deposit composition at the very low and high current densities studied, and exhibits a maximum of 28% at 27 mA cm^{-2}. The iron sulfate addition to the electrolyte does not cause any significant change on the current efficiency.

3.2. *Microstructure*

Figure 4 shows SEM micrographs of NiCu/Cu multilayers electrodeposited at -3.55 mA cm^{-2} for 1200 s and -70.97 mA cm^{-2} for 37.5 s in the electrolyte at pH 2.5, 3.0 and 3.5 from left to right. The Cu- and Ni-rich layers are easily distinguished. The dark regions represent the etched Cu-rich layers. The bright regions are the Ni-rich layers that remain unetched in the multilayer. The white areas that cover the top of the multilayer are resin residue from the etching process. The deposit at pH 2.5, contains 50 bilayers while the others, at pH 3.0 and 3.5, contain 20 bilayers each for a shorter plating time. The bilayer thickness is approximately 500 nm by inspection of the SEM micrograph and consistent with the calculated values when the current efficiency and composition is taken into account. In all deposits the

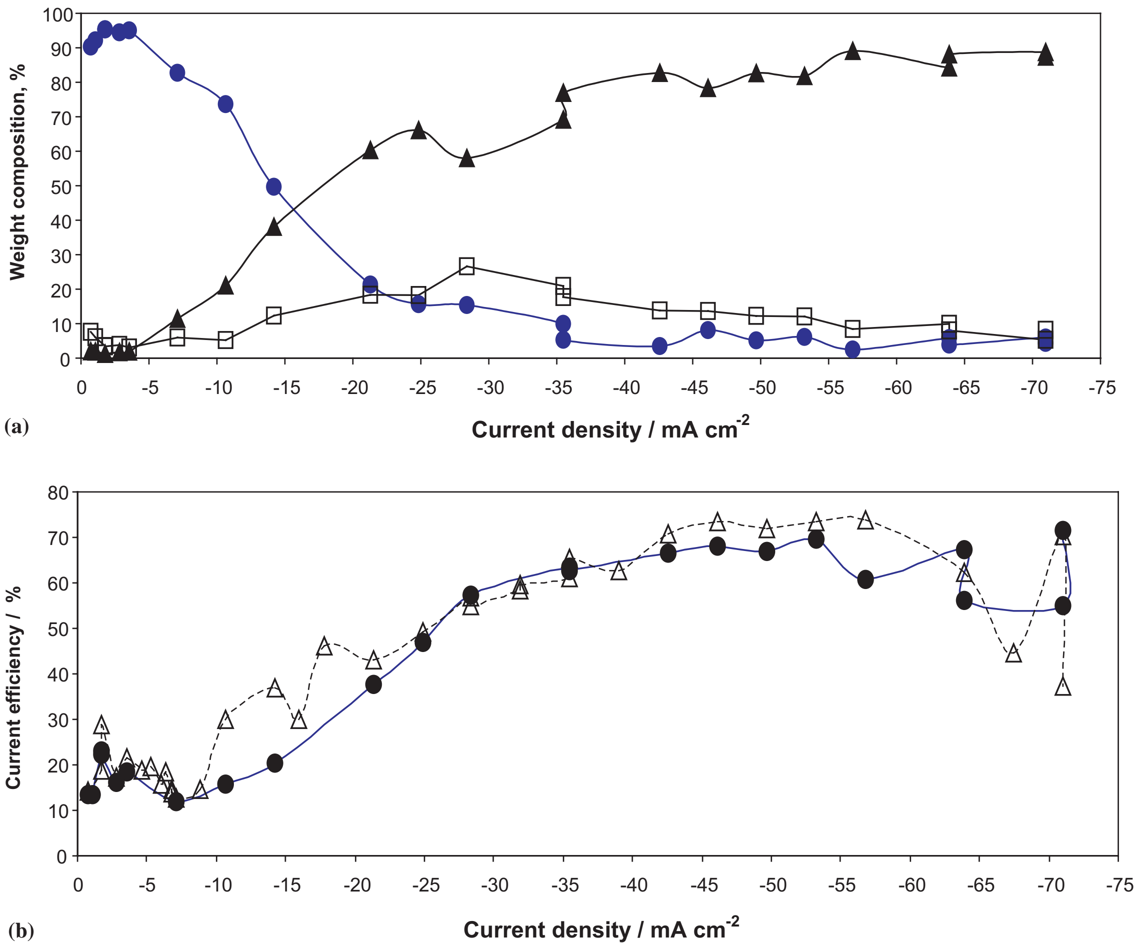

Fig. 3. NiCuFe (a) deposit composition at pH 3.0, Fe(□), Cu (●), Ni (▲); and (b) current efficiency, without Fe additive (△); with Fe additive (●).

multilayers exhibits a wavy profile on a macroscopic scale, due to the grain boundaries through the multilayer.

The Cu-rich layer current density was also examined. Keeping the Ni-rich layer deposition current density constant at -70.97 mA cm^{-2}, different current densities for the Cu-rich layer were used to prepare the multilayers at pH 3.0. The length of the Cu electrodeposition time was adjusted accordingly to keep the Cu-rich layer thickness constant, including the change of current efficiency. The multilayers fabricated with a current density for the Cu-rich layer of -0.71, and -1.8 mA cm^{-2} are shown in Figure 5(a) and (b). Compared with Figure 4(b), the waviness is slightly reduced as the applied Cu layer current density increased, consistent with literature studies [30], although not completely eliminated. Figure 5(c) is a magnification on a grain observed in the deposit plated with the Cu-rich layer current density at -1.8 mA cm^{-2} for pH 3.0 electrolyte. Comparing Figures 4(b) and 5, the grain

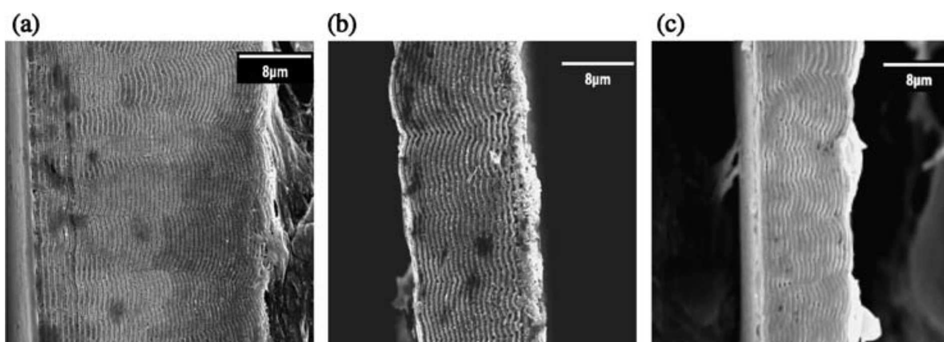

Fig. 4. SEM micrographs of NiCu/Cu multilayers at different electrolyte pH; current density of Cu: -3.55 mA cm^{-2} and of NiCu: -70.97 mA cm^{-2} at variable pH (a) 2.5, (b) 3.0, and (c) 3.5.

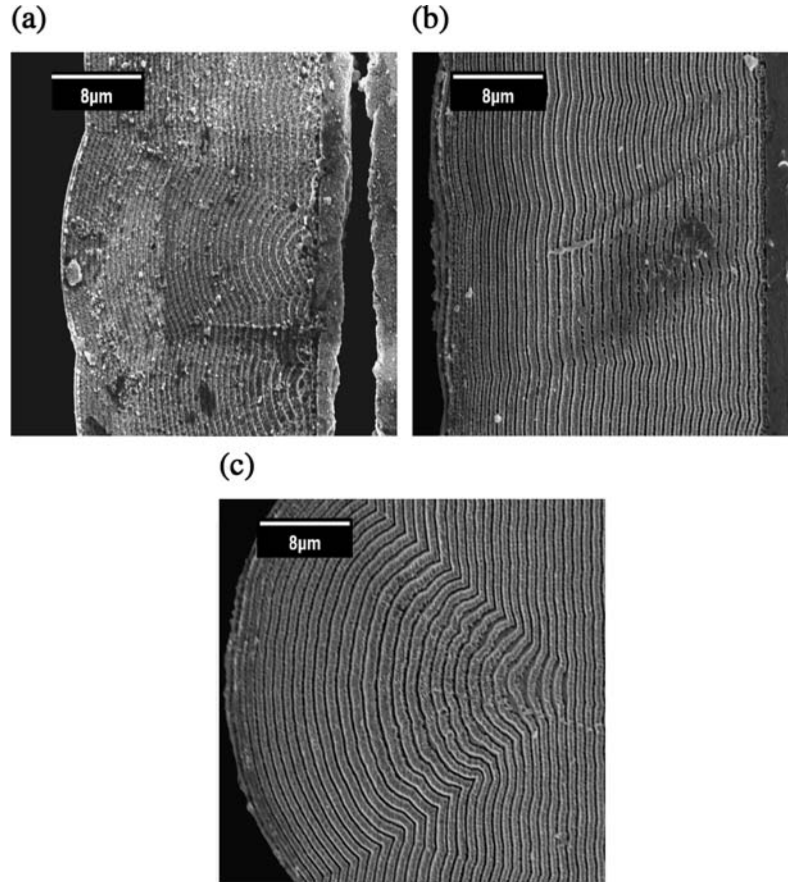

Fig. 5. SEM micrographs of NiCu/Cu multilayers at pH 3.0, with variable Cu current densities (a) −0.71, (b) −1.8 and (c) a single grain observed at −1.8 mA cm^{-2} for Cu. The NiCu current density layer was constant at −70.97 mA cm^{-2}.

growth can start not only from the substrate but also from the middle of the multilayer.

Figure 6(a) and (b) shows the influence of the multilayer when adding iron to the electrolyte. The multilayers consisted of 200 nm Cu- and Ni-rich layers each (400 nm bilayer) using pH 3.0 electrolyte with a Cu-rich layer current density at −1.8 mA cm^{-2} for 918 s without the iron addition and at 1174.8 s with the iron addition. The differences in time was to account for the difference in current efficiency observed in the multilayers. For the Ni-rich layer the current density was constant at −70.97 mA cm^{-2} layer for 15 s for both deposits in Figure 6(a) and (b). A slight reduction in the waviness of the multilayers containing iron was observed. When there was no iron present in the electrolyte, lower Cu-rich layer current densities exaggerated the waviness (Figures 4(b) and 5). Figure 7 (a) and (b) shows multilayers when the Cu-rich layer current

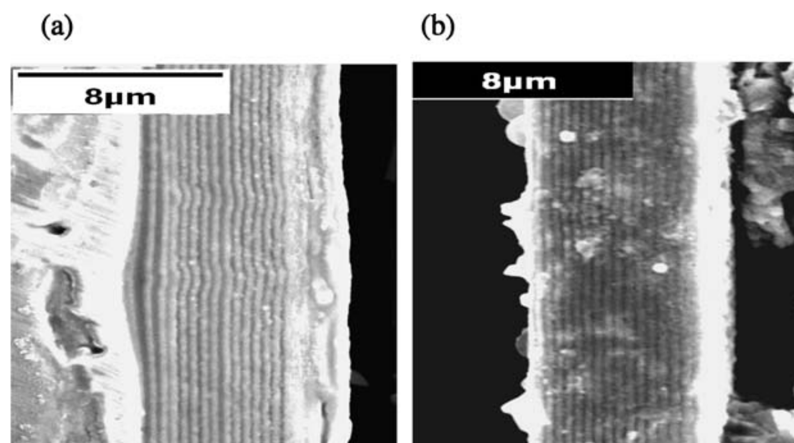

Fig. 6. SEM micrographs of (a) NiCu/Cu and (b) NiFeCu/Cu multilayers at pH 3.0; −1.8 mA cm^{-2} for Cu-rich layer; and −70.97 mA cm^{-2} for NiCu.

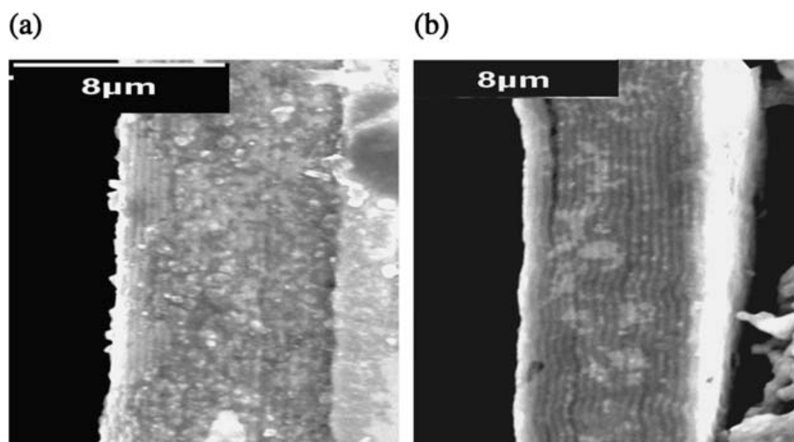

Fig. 7. SEM micrographs of NiFeCu/Cu multilayers at pH 3.0; (a) −0.71 and (b) −3.55 mA cm^{-2} for Cu-rich layer; and −70.97 mA cm^{-2} for Ni-rich layer.

density was −0.71 and −3.55 mA cm^{-2} in the iron containing bath. The bilayers are in general straighter compared to when no iron is present.

In Figure 8(a)–(c) are results of etched multilayers from the iron-containing electrolyte with smaller layer thickness plated (150 nm) achieved with different Cu-rich layer current densities at a constant charge of 0.41 and 0.70 C cm^{-2} for Cu-rich and NiFe-rich layers, respectively. The waviness characteristic does not arise. Figure 8(d) shows a higher magnification of a portion of a multilayer plated with a Cu-rich current density of −0.71 mA cm^{-2}. The etched portions (dark areas) are thinner than the calculated plated thickness, due to either a change in current efficiency compared to the steady-state analysis, or incomplete etching. Nevertheless, the Cu-rich layer is less than 100 nm.

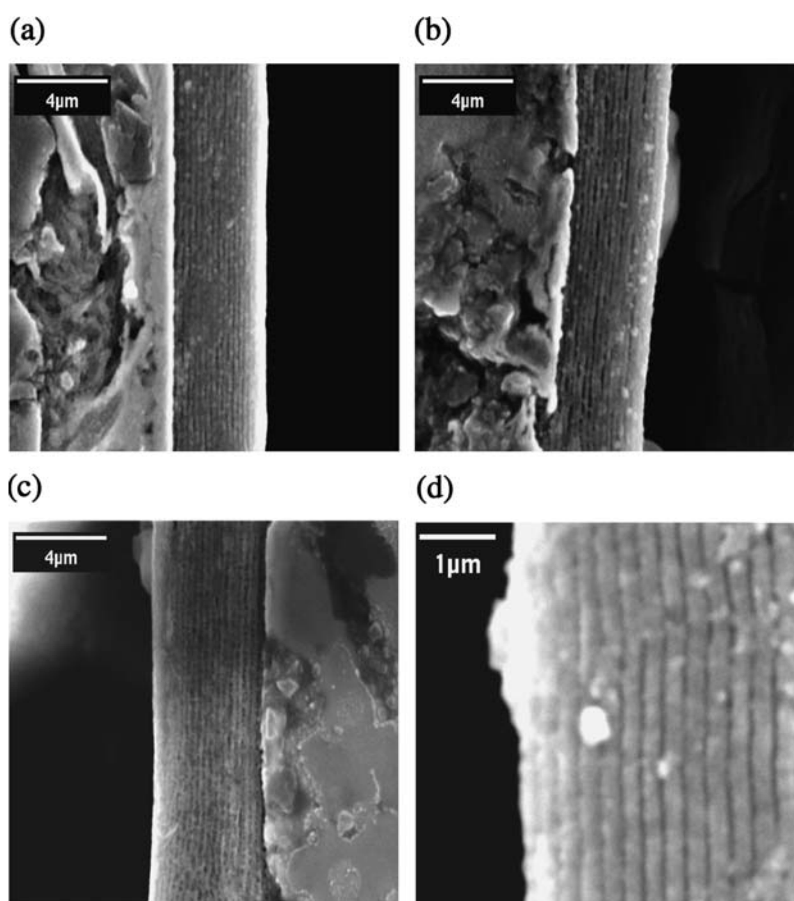

Fig. 8. Straight multilayered stamp with 150 nm layer thickness (a) −0.71, (b) −1.8, (c) −3.55 mA cm^{-2} for Cu-rich layer, and (d) −0.71 mA cm^{-2} for Cu at high magnification; −70.97 mA cm^{-2} for Ni-rich layer.

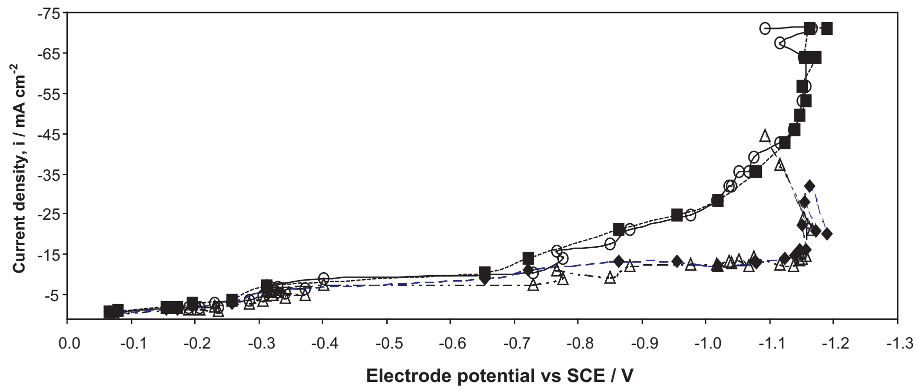

Fig. 9. Total current density, (○) no Fe; (■) with Fe and side reaction partial current density, (△) no Fe; (♦) with Fe at pH 3.0.

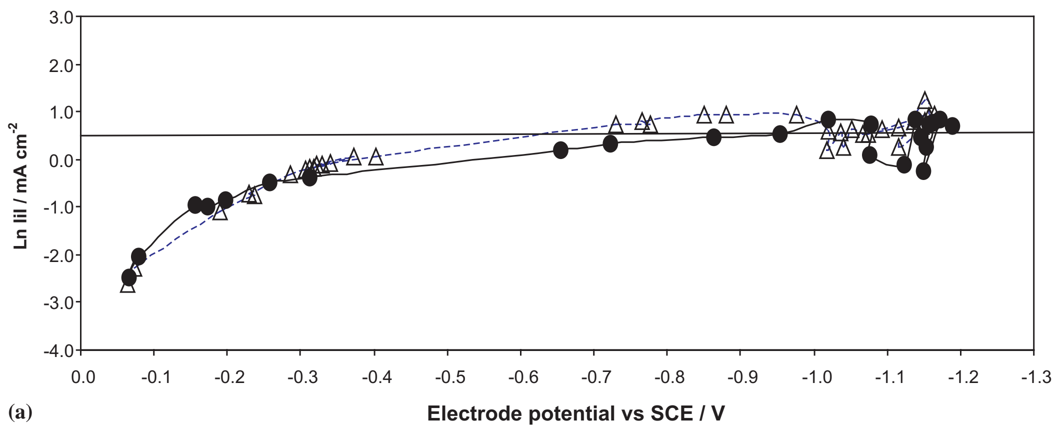

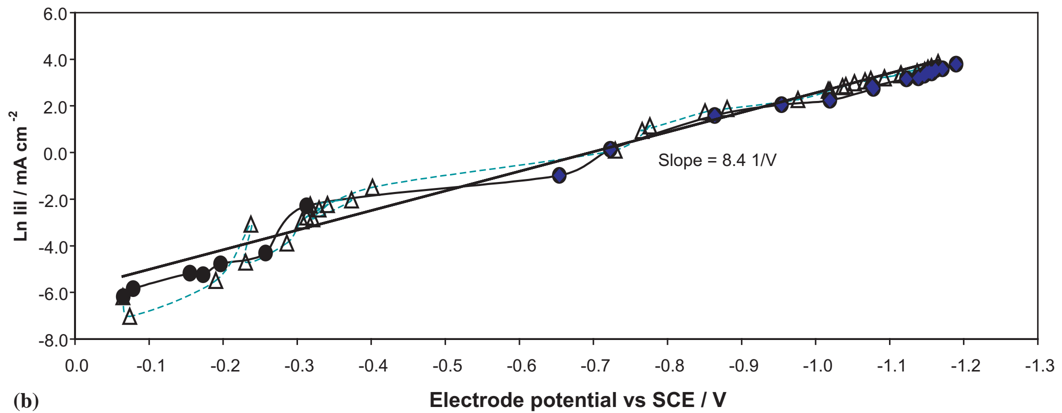

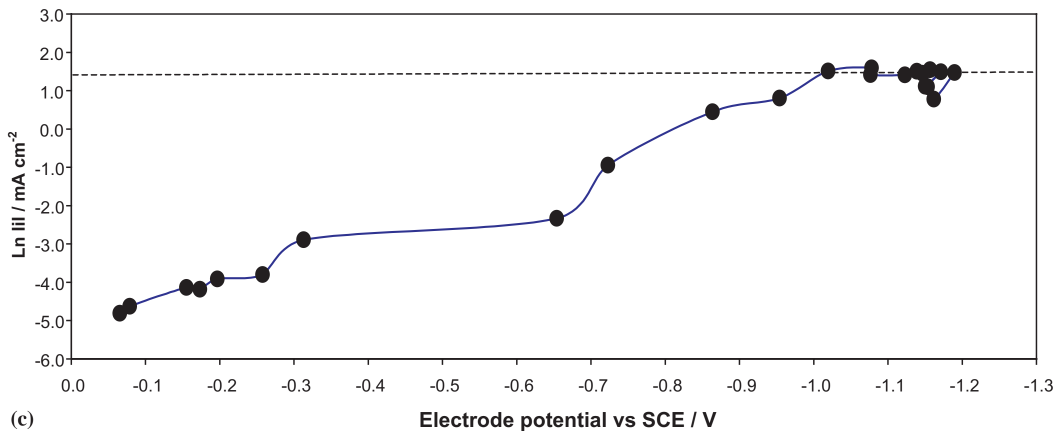

Fig. 10. Partial current densities from pH 3.0 electrolyte; (a) Cu (△) no Fe; (●) with Fe; (b) Ni (△) no Fe; (●) with Fe; (c) Fe.

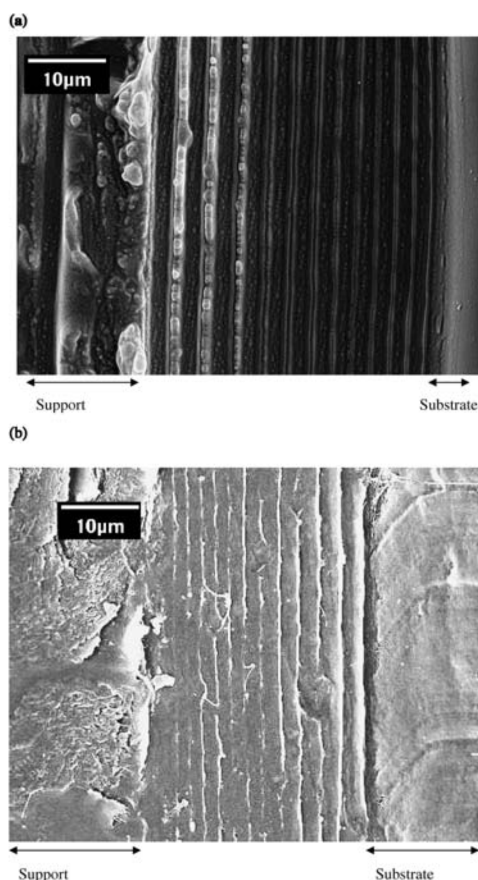

Fig. 11. Replicate multilayers of a 1000 nm layer-size in (a) Struer's rubber and (b) carbon-impregnated Teflon®.

3.3. *Partial current densities*

Figure 9 shows the total current density of the electrolyte with and without iron at pH 3.0. The small addition of iron does not affect the total polarization appreciably. The side reaction partial current density is also presented in Figure 9. At potentials more noble than −0.7 V vs SCE the side reactions represent an appreciable amount of the total current. In this range, the reactions that dominate are the reduction of oxygen and hydrogen evolution from proton reduction. At larger negative potentials than −1.1 V vs SCE the side reaction rises due to the reduction of water. Although the total current density and side reactions are the same with and without iron addition to the electrolyte, this does not imply that the partial current densities of Cu and Ni are constant. Therefore the partial current densities were compared with and without the Fe addition.

Figure 10 (a)–(c) shows the partial current densities of Cu, Ni and Fe, respectively, in the pH 3.0 electrolyte with and without iron. In Figure 10(a), the Cu limiting current densities are achieved after the potential reaches −0.7 V vs SCE. The iron addition does not contribute any significant effect on the copper's limiting current density at -1.6 mA cm^{-2}. Note that some of the Cu-rich layers in the multilayers shown in Figures 4, 7, and 8 were prepared exceeding the copper limiting current density; and that these Cu-rich alloys still are preferentially etched. In Figure 10(b) the Ni partial current density is compared with and without iron. Since NiFe deposition exhibits anomalous codeposition [31–33]. it is expected that the Ni rate may be inhibited by iron. Due to the small amount of iron in the electrolyte, the inhibition is barely discernable. The inverse Tafel slope for Ni, without the iron addition, is 8.4 V^{-1}. Figure 10(c) shows the reaction rate of Fe. The limiting current density is -4.1 mA cm^{-2}.

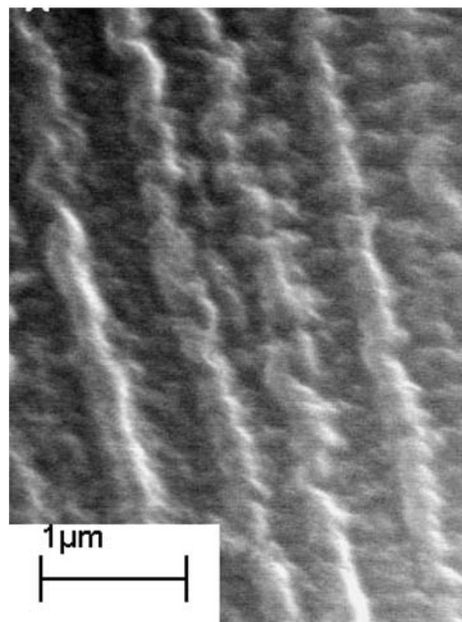

Fig. 12. SEM images of a PDMS cast of the layers from a 200 nm multilayer-etched sample.

3.4. *Replicates*

A multilayer stamp prepared from the NiCuFe electrolyte, pH 3.0, was used to replicate the image in rubber and in carbon-impregnated Teflon®. A larger layer size was chosen to more easily examine the replicates shown in Figure 11. The layer sizes of the master stamp were 1000 nm and it was not coated with Au for replication. In Figure 11, the raised regions (lighter contrast) correspond to the Cu-rich alloy region etched away in the master. Both the rubber and Teflon® reproduce the multilayer image. The rubber SEM shows regions where air was trapped in the metal master resulting in a non-uniform replicate particularly in the raised regions. The Teflon® was embossed by applying pressure and the image shows a more uniform impression.

Smaller dimensions were cast in PDMS. Figure 12 shows a replicated image with the embossed regions corresponding to the etched 200 nm copper layers. The layers are realizable and discrete. Currently, we are focusing on improving the replication and imaging at lower dimensions.

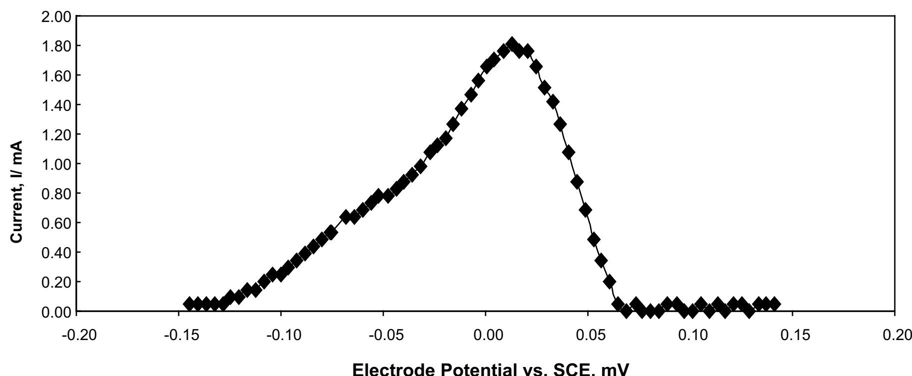

Fig. 13. Example stripping curve of alloy used to determine the current efficiency.

4. Conclusion

Compositionally modulated alloys were fabricated electrochemically and one layer preferentially etched to create a master stamp having sub-micron dimensions in NiCu/Cu and NiCuFe/Cu multilayered alloys. Electrolyte pH and Cu-layer current density were examined in order to create macroscopically straight layers, examined by SEM. The most successful master was created with the NiCuFe/Cu system at pH 3.0 electrolyte, −70.97 for Ni-rich layer and $-3.55\ \mathrm{mA\ cm^{-2}}$ for the Cu-rich layer. The multilayer impression was duplicated in a rubber, Teflon® and PDMS.

Acknowledgement

This work was support by the National Science Foundation, Grant # ECE-0202766.

References

1. Y. Hirai and Y. Tanaka, *J. Photopolymer Sci. Technol.* **15**(3) (2002) 474.
2. S.Y. Chou, *Sci. Spectra* **10** (1998) 38.
3. S. Zankovych, I. Maximov, I. Shorubalko, J. Seekamp, M. Beck, S. Romanov, D. Reuter, P. Schafmeister, A.D. Wieck, J. Ahopelto, C.M. Sotomayor Torres and L. Montelius, *Microelectron. Eng.* **67–68** (2003) 214.
4. K.D. Bird and M. Schlesinger, *J. Electrochem. Soc.* **142** (1995) L65.
5. E. Toth-Kadar, L. Peter, T. Becsei, J. Toth, L. Pogany, T. Tarnoczi, P. Kamasa, I. Bakonyi, G. Lang, A. Cziraki and W. Schwarzacher, *J. Electrochem. Soc.* **147** (2000) 3311.
6. P. Nallet, E. Chassaing, M.G. Walls and M.J. Hytch, *J. Appl. Phys.* **79** (1996) 6884.
7. Y. Jyoko, S. Kashiwabara and Y. Hayashi, *J. Electrochem. Soc.* **144** (1997) L5.
8. E. Chassaing, A. Morrone and J.E. Schmidt, *J. Electrochem. Soc.* **146** (1999) 1794.
9. L. Peter, A. Cziraki, L. Pogany, Z. Kupay, I. Bakonyi, M. Uhlemann, M. Herrich, B. Arnold, T. Bauer and K. Wetzig, *J. Electrochem. Soc.* **148** (2001) C168.
10. M. Alper, K. Attenborough, R. Hart, S.J. Lane, D.S. Lashmore, C. Younes and W. Schwarzacher, *Appl. Phys. Lett.* **63** (1993) 2144.
11. M. Alper, K. Attenborough, V. Baryshey, R. Hart and D.S. Lashmore, *J. Appl. Phys.* **75** (1994) 6543.
12. M. Alper, W. Schwarzacher and S.J. Lane, *J. Electrochem. Soc.* **144** (1997) 2346.
13. A.P. O'Keefe, O.I. Kasyutich, W. Schwarzacher, L.S. de Oliveira and A.A. Pasa, *Appl. Phys. Lett* **73** (1998) 1002.
14 O.I. Kasyutich, W. Schwarzacher, V.M. Fedosyuk, P.A. Laskarzhevskiy and A.I. Masliy, *J. Electrochem. Soc.* **147** (2000) 2964.
15. P.L. Cavallotti, D. Manara, R. Vallauri, A. Vicenzo, J. Machado da Silva and M.A. Sa, *in* L.T. Romankiw, S. Krognelb and C.H. Ahn (Eds), 'Magnetic Materials, Processes, and Devices', PC 98-20 (The Electrochemical Society Proceedings Series, Pennington, NJ, 1998), P.156.
16. E. Chassaing, P. Nallet and M.F. Trichet, *J. Electrochem. Soc.* **143** (1996) L98.
17. L.T. Romankiw and D.J. Olsen, *in* L.T. Romankiw and D.A. Hermon, Jr. (Eds), 'Magnetic Materials, Processes, and Devices', PV 90-8, (The Electrochemical Society Proceedings Series, Pennington, NJ, 1990), p. 339.
18. K. Attenborough, R. Hart, S.J. Lane, M. Alperand and W. Schwarzacher, *J. Magn. Magn. Mater.* **148** (1995) 335.
19. Q. Huang, D.P. Young, J.Y. Chan, J. Jiang and E.J. Podlaha, *J. Electrochem. Soc.* **149**(6) (2002) C349.
20. D. Simunovich, M. Schlesinger and D.D. Snyder, *J. Electrochem. Soc.* **141**(1) (1994) L10.
21. Ch. Bônhôte, Ph.D. Disseration, Ecole Polytechnique Federale de Lausanne, Switzerland (1998).
22. Y. Kita, Y. Kasai, S. Hashimoto, K. Iiyama and S. Takamiya, *Jap. J. Appl. Phys.* **40**(10) (2001) 5961.
23. R. Perez and J. Gomez, *Microscopy Research and Technique* **40**(1) (1998) 10.
24. T. Hasegawa, S. Aria, N. Kaneko and N. Shinohara, Annual Meeting of the Electrochemical Society of Japan Proceedings, 2E19, p. 89, (2001).
25. S. Aria, T. Hasegawa and N. Kaneko, *J. Electrochem. Soc.* **150**(11) (2003) C798.
26. S.D. Leith and Schwartz, *J. Micromech. Microeng.* **9** (1999) 97.
27. J.M. Brownlow, *J. Appl. Phys.* **38** (1967) 1440.
28. L.T. Romankiw, Proceedings of Second International Symposium on Magnetic Materials, Process and Devices, PV92-10 (The Electrochemical Society proceedings series, Pennington, NJ, 1992), p.367.
29. P.E. Bradley and D. Landolt, *Electrochim. Acta* **45**(7) (1999) 1077.
30. Ch. Bônhôte and D. Landolt, *Electrochim. Acta* **42**(15) (1997) 2407.
31. L. Giuliani and M. Lazzari, *Electrochimica Metallorum.* **3**(1) (1968) 45.
32. C. Brenner, 'Electrodeposition of Alloys' (A) (Academic Press, New York, 1963).

33. D. Landolt, *Electrochim. Acta* (D) **39** (8/9) (1994) 1075.

Appendix A

The current efficiency was determined by potentiodynamic stripping analysis. The electrolyte was a 0.10 M HCl aqueous solution, in a single compartment cell with a Ni counter electrode. The RDE cathode area was 0.282 cm^2 and the rotation rate was 1000 rpm. Figure 13 shows a representative stripping curve. The potential was swept from −150 to +150 mV vs SCE at 5 mV s^{-1}. The charge was determined by integration.